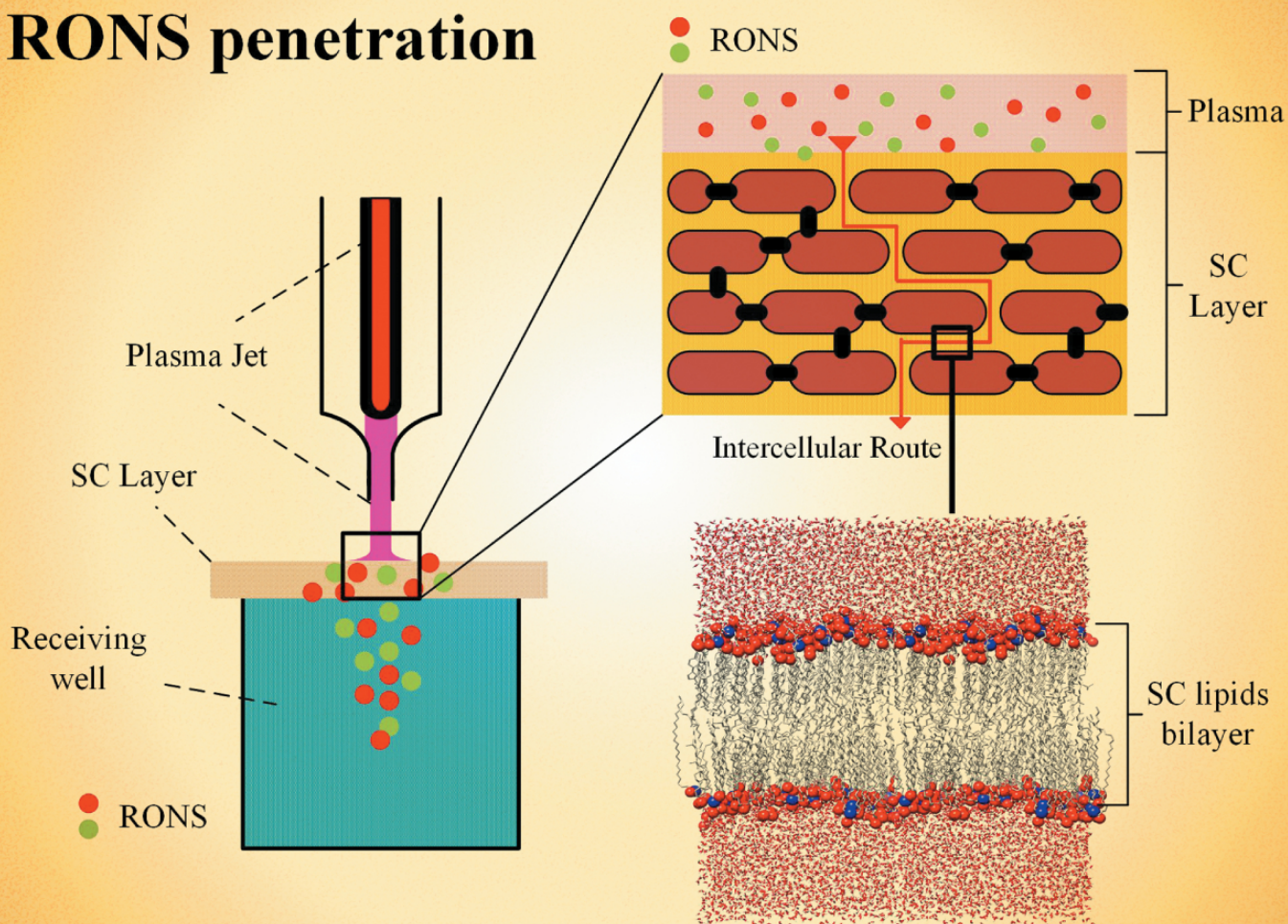Check for updates

PLASMA PROCESSES AND POLYMERS

The penetration of reactive oxygen and nitrogen species across the stratum corneum
Jiangwei Duan, Mingyu Ma, Maksudbek Yusupov, Rodrigo M. Cordeiro, Xinpei Lu, Annemie Bogaerts

RONS penetration

RONS · Plasma

SC Layer

Intercellular Route

Plasma Jet

SC Layer

Receiving well

RONS

SC lipids bilayer

Special Issue: Advanced Applications of Plasmas in Life Sciences
Guest Editors: Eloisa Sardella and Hiromasa Tanaka

WILEY-VCH

FULL PAPER

The penetration of reactive oxygen and nitrogen species across the stratum corneum

Jiangwei Duan[1,2,3] | Mingyu Ma[1] | Maksudbek Yusupov[3] |
Rodrigo M. Cordeiro[4] | Xinpei Lu[1,2] | Annemie Bogaerts[3]

[1]State Key Laboratory of Advanced Electromagnetic Engineering and Technology, School of Electrical and Electronic Engineering, Huazhong University of Science and Technology, Wuhan, China

[2]IFSA Collaborative Innovation Center, Shanghai Jiao Tong University, Shanghai, China

[3]Research Group PLASMANT, Department of Chemistry, University of Antwerp, Antwerp, Belgium

[4]Centro de Ciências Naturais e Humanas, Universidade Federal do ABC, Santo André, Santo André, São Paulo, Brazil

Correspondence
Xinpei Lu, State Key Laboratory of Advanced Electromagnetic Engineering and Technology, School of Electrical and Electronic Engineering, Huazhong University of Science and Technology, 430074 Wuhan, China.
Email: luxinpei@hotmail.com

Annemie Bogaerts, Research Group PLASMANT, Department of Chemistry, University of Antwerp, Antwerp-Wilrijk, Belgium.
Email: annemie.bogaerts@uantwerpen.be

Abstract

The penetration of reactive oxygen and nitrogen species (RONS) across the stratum corneum (SC) is a necessary and crucial process in many skin-related plasma medical applications. To gain more insights into this penetration behavior, we combined experimental measurements of the permeability of dry and moist SC layers with computer simulations of model lipid membranes. We measured the permeation of relatively stable molecules, which are typically generated by plasma, namely H_2O_2, NO_3^-, and NO_2^-. Furthermore, we calculated the permeation free energy profiles of the major plasma-generated RONS and their derivatives (i.e., H_2O_2, OH, HO_2, O_2, O_3, NO, NO_2, N_2O_4, HNO_2, HNO_3, NO_2^-, and NO_3^-) across native and oxidized SC lipid bilayers, to understand the mechanisms of RONS permeation across the SC. Our results indicate that hydrophobic RONS (i.e., NO, NO_2, O_2, O_3, and N_2O_4) can translocate more easily across the SC lipid bilayer than hydrophilic RONS (i.e., H_2O_2, OH, HO_2, HNO_2, and HNO_3) and ions (i.e., NO_2^- and NO_3^-) that experience much higher permeation barriers. The permeability of RONS through the SC skin lipids is enhanced when the skin is moist and the lipids are oxidized. These findings may help to understand the underlying mechanisms of plasma interaction with a biomaterial and to optimize the environmental parameters in practice in plasma medical applications.

RONS penetration
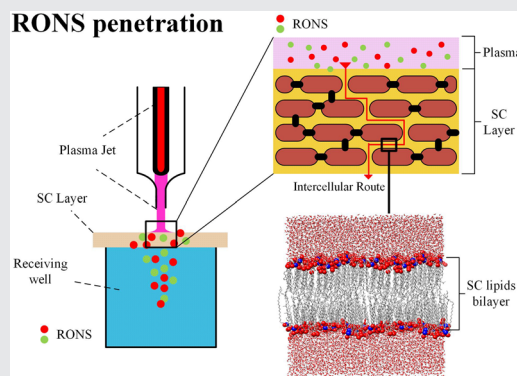
KEYWORDS

cold plasma, nonthermal plasma, penetration, reactive species, stratum corneum

Jiangwei Duan and Mingyu Ma contributed equally to this study.

----

1 | INTRODUCTION

Cold atmospheric plasma is gaining increasing interest in many medical applications, such as wound healing,[1–3] skin disease treatment,[4,5] and cancer therapy.[6–8] It is a cocktail that consists of various physical and chemical components, including electrons, ions, neutrals, strong electric field, heat, and ultraviolet light, which may influence the therapeutic effects. Among these components, the reactive oxygen and nitrogen species (ROS and RNS, or RONS) generated by the plasma are regarded as the main contributors to its therapeutic effects.[9] They include, among others, H_2O_2, OH, O, $^1O_2$, O_3, NO, NO_2, and HOONO, and the concentration of these plasma-generated RONS can vary, depending on the discharge and feed gas parameters. It should be noted that we also include relatively stable species such as NO_2^- and NO_3^- under the designation of RONS, because they are typical end products of RONS reactions.

RONS are able to affect the cell proliferation,[10] migration,[11] and apoptosis[12,13] via lipid oxidization,[14] DNA damage,[15,16] or cell-signaling activations.[17] These species are also able to stimulate the immune responses by regulating the release of immune-related factors[18] and affecting the immune cells.[19] However, in practice, for many skin-related applications, these reactive species must be delivered into the skin, reaching a deeper target, to achieve their therapeutic effects.[20] In this process, they need to penetrate through the stratum corneum (SC) first.

The SC is the outermost layer of the skin, which plays the most important role in the skin barrier function, preventing the penetration of compounds into the body via the epidermis. The structure of the SC is often described as a "brick-and-mortar" structure, in which the corneocytes represent the bricks and the lipids correspond to the mortar. The corneocytes are the dead and keratin-rich cells, which are surrounded by a mixture of intercellular lipids. These lipids are organized into a multilamellar structure that is the only continuous structure in the SC. There are two transepidermal penetration pathways for a molecule permeating through the SC layer: transcellular route and intercellular route. The transcellular route mainly penetrates through the corneocytes directly and the intercellular route mainly penetrates through the intercellular lipids. It is believed by many researchers that the intercellular route is the main penetration pathway for most of the components.[21] Besides, for the molecule permeating through an SC layer via the transcellular pathway, a partitioning through the keratin bricks and across the intercellular lipids is required. Thus, the intercellular lipids are important for both pathways, playing a major role in the barrier nature of the SC, even for the molecule permeating through the transcellular route.

It is reported that the major intercellular lipids of the SC are ceramides (CERs), free fatty acids (FFAs), and cholesterol (CHO).[22–24] To investigate the characters of the lipid mixture and the penetration of some components across the SC layer, the molecular dynamics (MD) simulations are widely used. In MD simulations, the SC lipid mixture is simplified in a lipid bilayer composed of CERs, FFAs, and CHO molecules. With the lipid bilayer model, the characters of the SC barrier and the penetration of some molecules are investigated successfully,[25–27] which indicates it is a useful tool and can even be used for drug designing in the drug delivery system.[28,29]

Considering the very strong barrier effects of the SC and the important role of RONS in plasma medical applications, it is essential to investigate the penetration process of RONS across the SC layer.[30] Thus, in this study, we carried out experiments and MD simulations to address these questions. Experimentally, we measured the long-lived species (H_2O_2, NO_3^-, and NO_2^-) generated by the plasma, penetrating through and stored in dry and moist SC layers. By means of MD simulations, we investigated the permeation processes of the main plasma-generated RONS (i.e., H_2O_2, OH, HO_2, O_2, O_3, NO, NO_2, N_2O_4, HNO_2, HNO_3, NO_2^-, and NO_3^-) across native and oxidized SC lipid bilayers.

2 | EXPERIMENTS

2.1 | Preparation of the SC samples

The SC samples (Figure 1b) are isolated from porcine ear skin (Figure 1a), which has similar characteristics as human skin and is usually used for dermatopharmacokinetic studies in vitro.[31,32] The subcutaneous fat of skin samples isolated from the ear was first removed, and then the samples were immersed in 0.25% trypsin–EDTA (Gibco) at 37°C for 48 hr. After the immersion, the SC layer was peeled off with tweezers. Finally, after washing with water and air-drying, the SC layers were instantly used as biological samples for the experiments.

2.2 | Experimental setup

Figure 2 illustrates the experimental setup. The fresh SC layer, which was dried by using bibulous paper or kept moist by putting 100 µl of water over it, covered the receiving well (volume: 360 µl, area: 0.32 cm²/well) and was treated by a plasma jet for different times (0, 5, 10, 15, 20 min). After plasma treatment, the concentration of
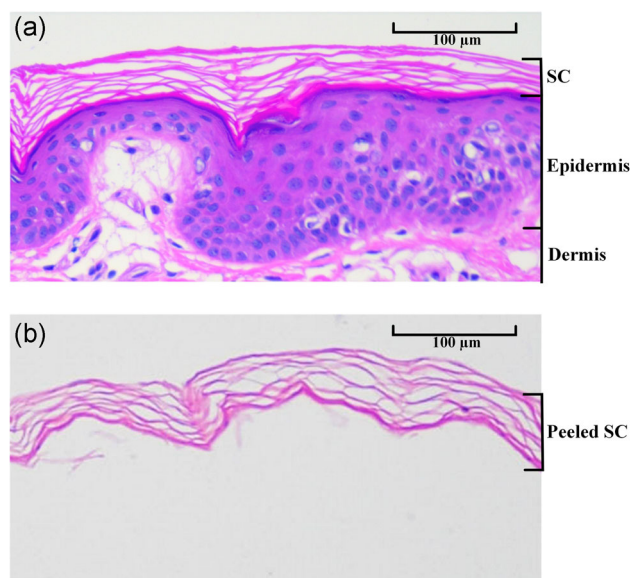
FIGURE 1 (a) Hematoxylin–eosin staining of normal porcine ear skin, showing the SC, epidermis, and a part of the dermis. (b) The intact SC layer was used in this experiment, which was peeled from the normal porcine ear skin. SC, stratum corneum

H_2O_2, NO_3^-, and NO_2^-, dissolved into the receiving well and stored in the SC layer, was measured immediately. Three fresh SC layers were used for the statistical analysis for every treatment time.

The parameters of the plasma jet were adjusted carefully to avoid the destruction of the SC layer. An alternating current with a peak-to-peak voltage of 15 kV and a frequency of 1 kHz was applied to generate plasma. The gas flow was a mixture of helium flow at 2 L/min and oxygen flow at 10 ml/min. The distance between the jet nozzle and the surface of the SC layer was 1 cm.

2.3 | Preparation of the SC sample extracts

The extracts of SC samples were prepared to measure the RONS stored in the SC layer after plasma treatment. The samples were ground by manual quartz grinders with 1-ml precooling water, and then the suspensions were centrifuged at 10,000 rpm for 5 min. The concentrations of H_2O_2, NO_3^-, and NO_2^- were measured in the supernatant liquid.
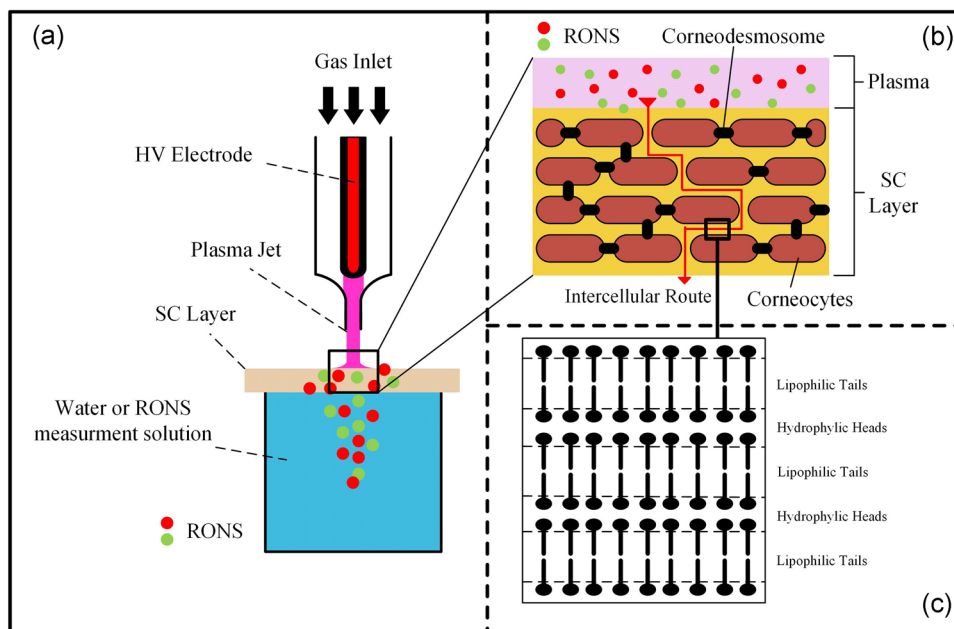

FIGURE 2 (a) The schematic diagram of the experimental setup. A fresh dry or moist SC layer was put on a receiving well and treated with a plasma jet. After plasma treatment, the concentration of H_2O_2, NO_3^-, and NO_2^-, penetrating through and stored in the SC layer, was measured. For H_2O_2 and NO_3^- measurement, the liquid in the receiving well was pure water (pH 7); for NO_2^- measurement, the liquid in the receiving well was Griess reagent (pH < 7), because NO_2^- is not very stable. (b) The "brick-and-mortar" structure of the SC. The corneocytes (bricks) are embedded in the matrix of special lipids (mortar) that consist of mainly ceramides, free fatty acids, and cholesterol,[22–24] and most of the components permeate through the SC by the intercellular route (mortar). (c) The highly ordered structure of the lipid matrix, consisting of stacked lipid layers. HV, high voltage; RONS, reactive oxygen and nitrogen species; SC, stratum corneum

2.4 | RONS measurements

The concentrations of H_2O_2, NO_3^-, and NO_2^- were measured after plasma treatment by the following methods.[33,34]

H_2O_2 was measured with Hydrogen Peroxide Assay Kit (Beyotime, China). A mixture of $100\,\mu l$ of test solutions and $100\,\mu l$ of the liquid sample was incubated at room temperature for 30 min and measured immediately with a microplate reader at a wavelength of 570 nm. The detection limit was $1\,\mu M$.

NO_3^- was measured with Nitric Oxide (NO) Assay Kit (nitrate reductase method; Nanjing Jiancheng Bioengineering Institute, China) according to the protocol. NO_3^- was transformed into NO_2^- induced by nitrate reductase, and then the NO_2^- concentration was measured by the Griess reagent with a microplate reader at a wavelength of 550 nm.

NO_2^- was measured with Nitrite Assay Kit (Nanjing Jiancheng Bioengineering Institute), which is a kind of Griess reagent. For NO_2^- penetration detection, the test solution was directly transferred to the receiving wells. For measuring the NO_2^- in the SC samples, a mixture of $100\,\mu l$ of the test solution and $100\,\mu l$ of the liquid sample was placed at room temperature for 15 min. The colorimetric results were measured at 550 nm by a microplate reader, and the detection limit was $1\,\mu M$.

2.5 | Statistical analysis

All of the experiments were performed in triplicate. The results are presented as mean $\pm$ standard deviation.

3 | COMPUTER SIMULATIONS

3.1 | Preparation of the model systems

To have an atomic-scale understanding of the permeation of different RONS across the native SC layer and to investigate the effects of oxidation induced by plasma on the RONS translocation, we performed MD simulations. Among the lipid composition of the SC layer, the polyunsaturated fatty acid component is particularly susceptible to peroxidation and can undergo significant change, and oxidized cholesterol (5α-CH) is the predominant oxidized species that is responsible for the structural changes.[35] Thus, 5α-CH was chosen to build the oxidized SC lipid bilayer. Native and 100% oxidized skin lipid bilayer models were built, based on literature.[35,36] Specifically, the model systems in our simulations contain a certain number of lipid molecules, such as CER, FFA, CHO, and 5α-CH molecules, where the latter was used in our oxidized model system (see Figure 3a).

The initial structures of the model lipid bilayers were constructed by the PACKMOL package.[37] Both the native and oxidized lipid bilayers contain 52 CERs and 52 FFAs, as well as either 50 CHOs (in the native system) or 50 5α-CHs (in the oxidized system), equally distributed in both layers and covered with water molecules on top and at the bottom (see Figure 3b). Thus, the CHOs of the native system are entirely (100%) oxidized into 5α-CH in the oxidized system.

All the MD simulations were performed using the GROMACS 2018.3 package.[38] The GROMOS-type force field parameters were used for the interatomic interactions. The parameters of CER, FFA, and CHO were based on the study of Berger et al.[39] and Höltje et al.[40] The parameters of 5α-CH were derived from the study reported by Neto and Cordeiro.[41] The RONS parameters were obtained from the studies reported in References [42–45]. It is noted that HNO_2 has two configurations, that is, *trans*-HONO and *cis*-HONO, and both of them were studied in this study. The simple point charge model was used for the water molecules.

It should be noted that the force field used in the study is a nonreactive force field, which does not allow the breaking and formation of bonds; therefore, chemical reactions of the RONS with the lipids and water could not be included during the simulations. However, these MD simulations can provide some valuable insights for the permeabilities of RONS, based on their physical characters, including the charge of particles, the polarity of particles, the Van der Waals interactions, and even the H-bond interactions.

The native and oxidized skin lipid bilayers were first energy-minimized with the steepest descent algorithm and then equilibrated with the isothermal–isobaric (NPT) ensemble for 50 ps at 1 bar and 310.15 K, using a time step of 0.5 fs, to release the bad contacts in the systems. Then, again the NPT ensemble was run for 150 ns at 1 bar and 310.15 K, using a time step of 2 fs. The temperature was controlled by the Nose–Hoover thermostat, combined with a coupling constant of 0.5 ps, and the pressure was controlled by the semi-isotropic Parrinello–Rahman barostat, combined with a coupling constant of 2 ps and compressibility of $4.5 \times 10^{-5}\,bar^{-1}$. The cut-off distance for the van der Waals interactions was set at 1.0 nm, and the particle mesh Ewald method was applied to calculate electrostatic interactions. Periodic boundary conditions were applied in all three directions.
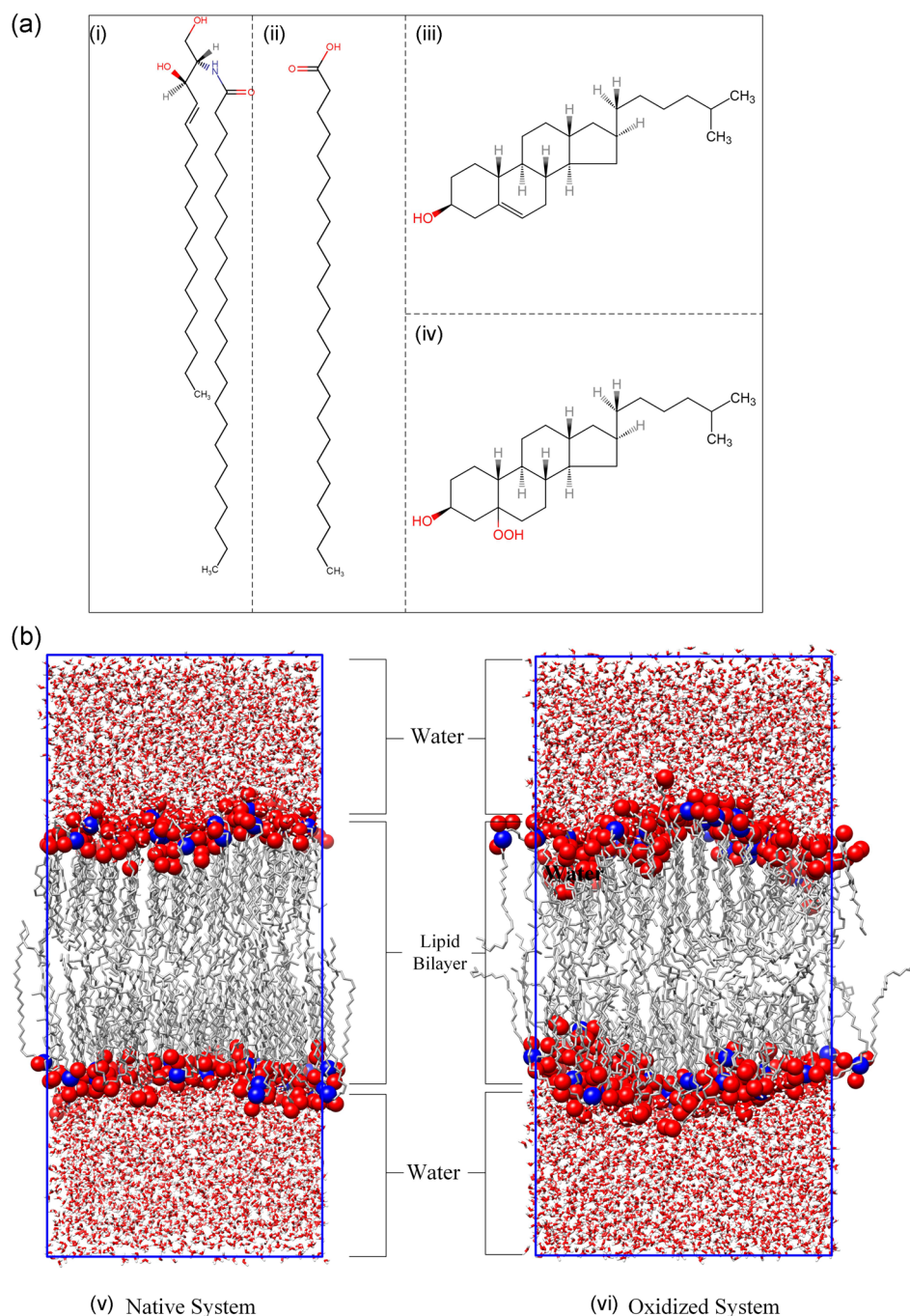
FIGURE 3 (a) Skin lipid molecules used to build the model systems: (i) ceramide (CER), (ii) free fatty acid (FFA), (iii) cholesterol (CHO), and (iv) oxidized cholesterol (5α-CH). (b) The model systems used in our simulations: (v) the native system consisting of 52 CERs, 52 FFAs, 50 CHOs, and 5,120 water molecules; and (vi) the oxidized system containing 52 CERs, 52 FFAs, 50 5α-CHs, and 5,120 water molecules. As is clear, the native and oxidized model systems differ only in (un)oxidized CHO molecules. The O atoms of all lipid molecules and N atoms of CERs are marked with red and blue, respectively. For clarity, these atoms are depicted with bigger beads

3.2 | Calculation of the free energy profiles (FEPs)

To investigate the transport of different RONS across the native and oxidized SC layers, the permeation FEPs of RONS (i.e., H_2O_2, OH, HO_2, O_2, O_3, NO, NO_2, N_2O_4, HNO_2, HNO_3, NO_2^-, and NO_3^-) through the native and preoxidized skin lipid bilayers were calculated using the umbrella sampling (US) method. Specifically, to obtain the average FEP of each electroneutral RONS (i.e., H_2O_2,

OH, HO_2, O_2, O_3, NO, NO_2, N_2O_4, HNO_2, and HNO_3) for each model system, five structures of lipid bilayers were used, which were derived from the last 50 ns of equilibration runs. For calculation of each individual FEP, 176 US windows were defined in the z axis (i.e., along the bilayer normal), separated by 0.5 Å. In each US simulation, 32 individual particles (e.g., H_2O_2) were inserted into the system, distributed over eight planes along the z axis (i.e., four particles in each plane) and separated by 1.1 nm from each other in the z axis. Thus, by performing 22 (176/8) US simulations, we obtained four FEPs, each ranging from −4.4 to 4.4 nm in the z axis. The movement of the inserted particles was restrained along the z axis by a harmonic bias with a force constant of 2,000 kJ·mol^{-1}·nm^{-2}. They were also restrained to move in the xy plane by applying the flat-bottomed position restraint, with a radius of 0.5 nm and a force constant of 1,000 kJ·mol^{-1}·nm^{-2}. Thus, in this way, we were able to reduce computational costs. Each US simulation lasted 20 ns and the last 10 ns were used as sampling time (i.e., for the collection of data). It should be noted that this time was sufficient to obtain symmetric FEPs (i.e., symmetric to the center of the bilayer), which are indicative of proper convergence of the free energy simulations. In total, the FEP of each electroneutral RONS was obtained from 110 (5 × 22) US simulations and averaged over 20 (5 × 4) individual FEPs. The FEPs were constructed applying a periodic version of the weighted histogram analysis method (WHAM)[46] by using the gmx wham tool of GROMACS. In the case of HNO_2, two different sets of simulations were compared, each one starting from either the *cis* or the *trans* configuration of HNO_2 and allowing transitions to occur.

We cannot use the same procedure for the ions (NO_2^- and NO_3^-) as applied above for the electroneutral RONS, as too many ions in the system (i.e., 32) lead to a disruption of the lipid model systems. Indeed, our test simulations showed the destruction of the bilayer systems. To solve this problem, we applied the following procedure for the ions. To calculate the FEPs of the ions (NO_2^- and NO_3^-) across the SC layers, we used three structures of lipid bilayers (i.e., three for the native and three for the oxidized system), derived from the last 50 ns of equilibration runs. For each US simulation, the starting structures (i.e., US windows) were obtained by pulling the center of mass of each ion across the lipid bilayers with a force constant of 2,000 kJ/mol and a slow pulling rate of 0.0001 nm/ps. Thus, in each US simulation, we used a single target anion, which does not lead to a disturbance of the system. To keep the system electrically neutral, Na$^+$ was added to the system by replacing the water molecule randomly in each US simulation. For one individual FEP calculation, 89 US windows were defined,

separated by 1 Å along the z axis. The FEPs were again constructed by the WHAM method.[46] Each US simulation lasted 20 ns, and the last 10-ns simulation time was used for the construction of the FEP. In total, 267 (3 × 89) US simulations were carried out for each ion to obtain the averaged FEP.

3.3 | Calculation of the area per lipid (APL) and bilayer thickness

The average APL and the average thickness of both native and oxidized bilayers were calculated by the GridMAT-MD package.[47] Specifically, the APL was determined by dividing the surface area of the SC bilayer by the total number of lipids (including CHO/5α-CH) of one layer, that is, $L_x \times L_y/77$, where L_x and L_y are the x and y dimensions of the bilayer, respectively, and 77 is the number of lipids present in one layer. The bilayer thickness was determined by averaging all distances (z components) between the O atoms of the two opposite layers of the SC bilayer. The last 50 ns of the equilibration simulations were used for obtaining the average APL and bilayer thickness.

4 | RESULTS AND DISCUSSION

4.1 | H_2O_2 measurement

The concentrations of H_2O_2 permeating across and stored in the SC layer after different plasma treatment times are presented in Figure 4. The results show that, in the absence of an SC layer, the concentration of H_2O_2 in the receiving well increases with treatment time, and it is up to $285.7 \pm 13.3 \, \mu M$ after 20-min plasma treatment (see Figure 4a). However, no H_2O_2 signals can be measured after plasma treatment, when the receiving well is covered with a dry SC layer. On the contrary, when the receiving well is covered by a moist SC layer, few H_2O_2 signals can be measured in the receiving well after 15-min ($1.6 \pm 0.3 \, \mu M$) and 20-min ($2.7 \pm 0.2 \, \mu M$) plasma treatment (see Figure 4a). Thus, H_2O_2 generated by the plasma jet cannot permeate across the dry SC layer and slightly permeates across the moist SC layer at a long treatment time under the experimental conditions used in this study. The number of H_2O_2 molecules stored in the SC layer after plasma treatment is shown in Figure 4b. As is clear, the amount of H_2O_2 remaining in the SC layer increases with treatment time, and more H_2O_2 molecules are stored in the SC layer when it is moist. For example, after 20-min plasma treatment, the density of H_2O_2 stored in the moist SC layer is $84.3 \pm 10.8 \times 10^{14} \, cm^{-2}$, which is about two
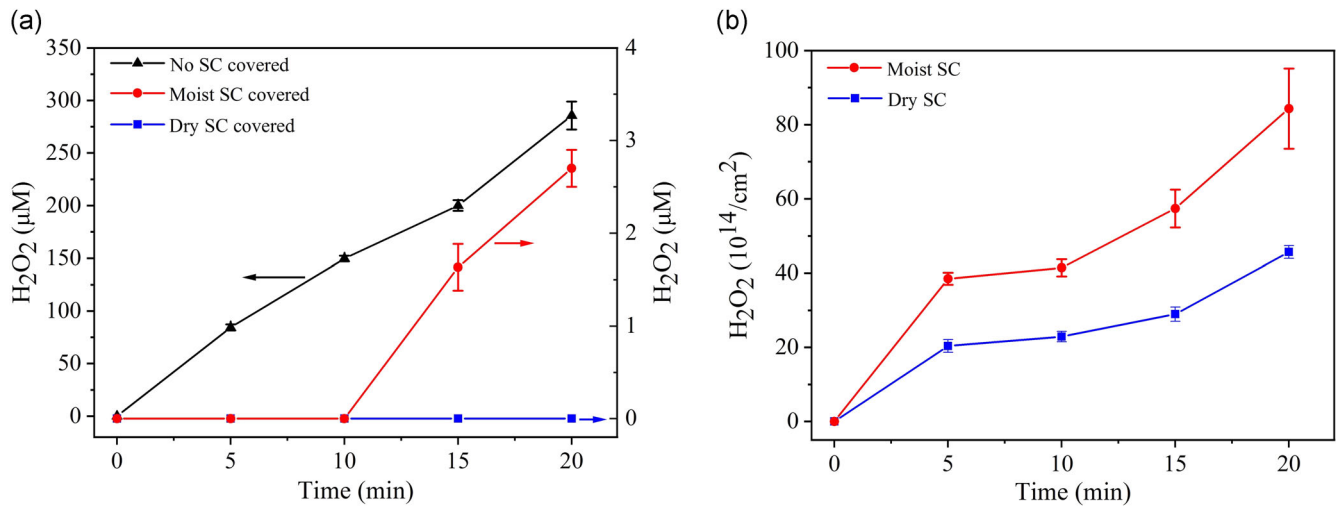
FIGURE 4 (a) The concentration of H_2O_2 in the water-containing receiving well after plasma treatment, when not covered by SC and when covered by either moist or dry SC. (b) The number of H_2O_2 molecules per square centimeter left in the SC layer after plasma treatment, for either moist or dry SC. SC, stratum corneum

times higher than the density of H_2O_2 stored in the dry SC layer ($45.7 \pm 1.7 \times 10^{14} \, cm^{-2}$), see Figure 4b.

4.2 | NO_3^- measurement

The concentration of NO_3^- in the receiving well (i.e., after penetrating the SC layer) and that stored in the SC layer also increases with increasing plasma treatment time (Figure 5). As is clear from Figure 5a, after 20-min plasma treatment, the concentration of NO_3^- permeating across the dry and moist SC layer is 3.6 ± 0.3 and $4.2 \pm 0.2 \, \mu M$, respectively, which is about one-ninth or one-eighth of the NO_3^-

concentration measured in the absence of an SC layer ($31.6 \pm 2.7 \, \mu M$). Furthermore, the density of NO_3^- stored in the moist SC layer is slightly higher than that in the dry SC layer (see Figure 5b). For example, after 20-min plasma treatment, the density of NO_3^- stored in the moist SC layer is $55.6 \pm 4.6 \times 10^{14} \, cm^{-2}$, whereas it is $42.6 \pm 2.7 \times 10^{14} \, cm^{-2}$ in the dry SC layer.

4.3 | NO_2^- measurement

The concentration of NO_2^- in the receiving well (i.e., after penetrating the SC layer) and that stored in the SC layer
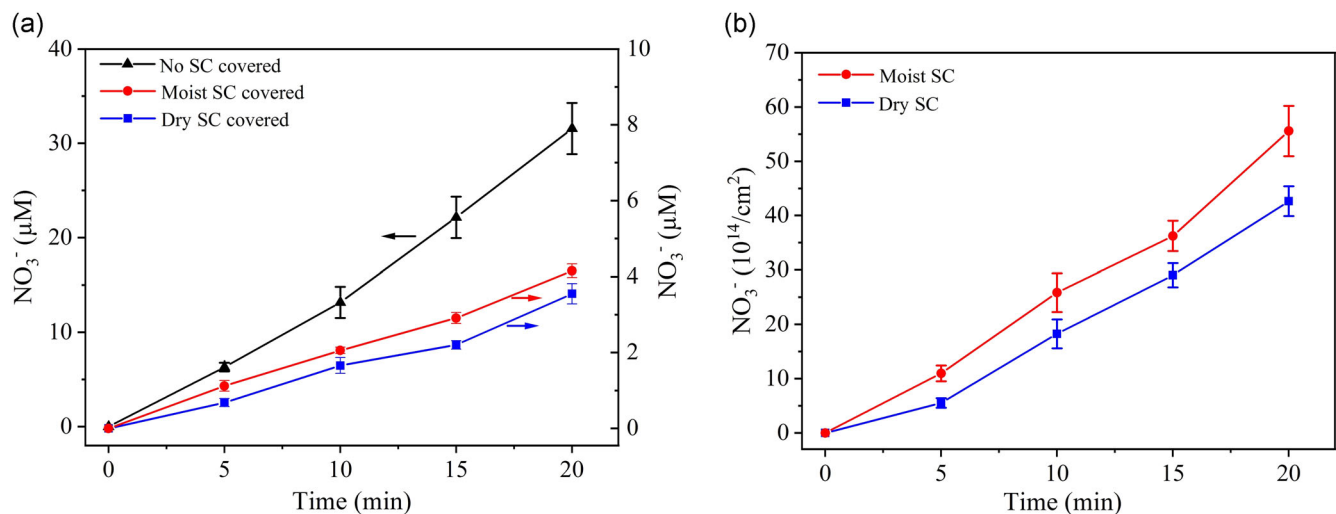

FIGURE 5 (a) The concentration of NO_3^- in the water-containing receiving well after plasma treatment, when not covered by SC and when covered by either moist or dry SC. (b) The number of NO_3^- molecules per square centimeter left in the SC layer after plasma treatment, for either moist or dry SC. SC, stratum corneum

FIGURE 6 (a) The concentration of NO_2^- in the water-containing receiving well after plasma treatment, when not covered by SC and when covered by either moist or dry SC. (b) The number of NO_2^- molecules per square centimeter left in the SC layer after plasma treatment, for either moist or dry SC. SC, stratum corneum
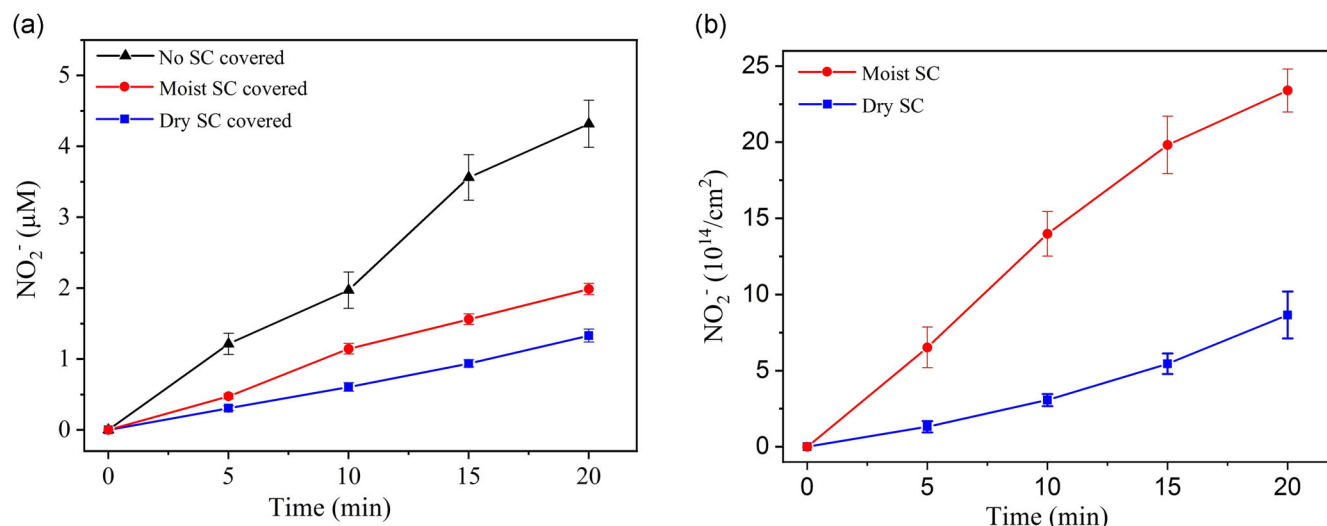
after different plasma treatment times is shown in Figure 6. In all conditions (i.e., with and without SC layer covering the well), the concentration of NO_2^- in the receiving well is about several micromolars, and it increases with treatment time. When the receiving well is covered with the SC layer, the concentration of NO_2^- permeating across this layer is $1.3 \pm 0.1\,\mu M$ (dry SC layer) or $2.0 \pm 0.1\,\mu M$ (moist SC layer) after 20-min plasma treatment, which is around one-third or a half of the NO_2^- concentration measured without the SC layer (i.e., $4.3 \pm 0.3\,\mu M$, see Figure 6a). Furthermore, the density of NO_2^- stored in the SC layer increases with plasma treatment time, and more NO_2^- is stored in the moist SC layer, compared with the dry SC layer (see Figure 6b). For example, after 20-min plasma treatment, the density of NO_2^- stored in the moist SC layer (i.e., $23.4 \pm 1.4 \times 10^{14}\,cm^{-2}$) is about three times higher than that in the dry SC layer (i.e., $8.7 \pm 1.6 \times 10^{14}\,cm^{-2}$).

Thus, from Figures 4–6, we can conclude that the permeabilities of the plasma-generated long-lived species (H_2O_2, NO_3^-, and NO_2^-) are different. H_2O_2 cannot penetrate across the dry SC, and it slightly penetrates through the moist SC at a long plasma treatment time. NO_3^- and NO_2^- can penetrate the SC in both dry and moist conditions. All the species can be stored in the SC layer, which is enhanced in the case of a moist SC layer.

4.4 | The effect of moisture of the SC layer on the RONS penetration and storage

The results of the previous section indicate that more RONS, especially H_2O_2, can penetrate through and be

stored in the moist SC layer than in the dry SC layer at a long treatment time. This may be caused by the different amounts of H_2O_2 produced in these layers and by the different permeation efficiencies of RONS in these two layers.

In a cold plasma jet, H_2O_2 is mainly formed by the recombination of OH radicals that are created upon dissociation of water molecules (see Reactions 1 and 2 below).[48,49] Hence, the water molecules are the crucial source for the generation of H_2O_2. It is reported that the H_2O_2 concentration in a cold plasma jet increases linearly with increasing humidity of the feed gas.[50] In our experiments, more H_2O_2 is produced on the top surface of the moist SC layer than that of the dry SC layer, causing more H_2O_2 penetration and storage in the moist SC layer (see Figure 4).

$$H_2O + P \rightarrow \bullet OH + \bullet H + P, \qquad (1)$$

$$\bullet OH + \bullet OH + M \rightarrow H_2O_2 + M, \qquad (2)$$
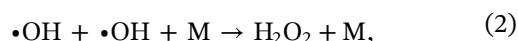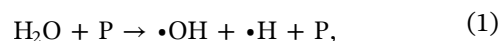
where P is an energetic particle (e.g., an electron or an excited helium atom) and M is an arbitrary collision partner (e.g., helium).

However, the moisture of the SC may also influence the penetration of other RONS. Previous research indicates that aqueous plasma-activated species penetrate mouse skin more easily than gaseous plasma-activated species, which was attributed to the different penetration pathways.[51] In the drug penetration field, retention of water in the skin can enhance the penetration of most of drugs, which may result from an increase in the SC hydration and swelling of corneocytes.[52] When the SC

layer is moist, the gaseous plasma-activated species convert into aqueous species at first and then penetrate through the SC layer, causing more RONS permeation than the direct gaseous plasma-activated species permeation (i.e., when the SC layer is dry). Thus, our results indicate that the bioeffects induced by cold plasma may be enhanced when the surface of the skin is moist.

4.5 | Penetration of different RONS

As mentioned in Section 1, various ROS and RNS are generated by the plasma jet, and they are regarded as the main contributors to the plasma medicine applications. According to the literature,[30,53] the most relevant ROS in plasma are atomic oxygen (O), singlet delta oxygen ($^1O_2$), superoxide (O_2^-), ozone (O_3), hydroxyl radicals (OH), and hydrogen peroxide (H_2O_2), whereas the most relevant RNS are nitric oxide (NO), nitrogen dioxide (NO_2), and peroxynitrite ($ONOO^-$). Nitrite (HNO_2/NO_2^-) and nitrate (HNO_3/NO_3^-) can also be generated as stable end products of RONS reactions. Some of these RONS (such as O and OH) exhibit strong oxidative properties, causing modification of lipids, proteins, and DNA, resulting in alterations in cells. Other RONS (like NO) act as the regulator of the cellular function, affecting the cell proliferations or immune responses.[54,55] When the skin is exposed to plasma, the RONS in the plasma should penetrate through the SC layer, reaching the deeper target, to achieve its therapeutic goal.

Previous research studies have indicated that short-lived RONS hardly penetrate through the SC layer due to their strong reactive character, resulting in a half-life time of several nanoseconds.[30] However, long-lived RONS have a longer half-life time, but they can also be consumed and trapped by the SC layer.

To quantize the effects of SC layer on the long-lived RONS penetration, we calculated the blocking ratio of the moist SC layer and dry SC layer with the following formula:

$$k_b = \left(1 - \frac{c_1}{c_2}\right) \times 100\%,$$

where k_b is the blocking ratio of the SC layer for a specific reactive species; c_1 is the concentration of a specific reactive species in the receiving wells after plasma treatment when the wells were covered with the SC layer; c_2 is the concentration of a specific reactive species in the receiving wells when there was no SC layer covering the wells. It should be noted that the blocking ratio k_b, in general, indicates the effects of SC layer on the RONS penetrations, compared with situations in which there was no SC layer coverage. The contributions of RONS productions, the RONS consumption by SC layer, and the different permeabilities of RONS across the SC layer are all reflected in the blocking ratio.

The blocking ratios of moist SC layer and dry layer on long-lived RONS after 20-min plasma treatment are presented in Table 1, which shows that approximately 99.1% of H_2O_2 is blocked by the moist SC layer and almost all of them are blocked from permeation by the dry SC layer. For the penetrations of NO_3^- ions, it is clear from Table 1 that 86.7% of NO_3^- is blocked by the moist SC layer and 88.6% is blocked by the dry SC layer. Similarly, for the NO_2^- penetration, 53.5% of NO_2^- is blocked by the moist SC layer, whereas 69.8% is blocked by the dry SC layer.

Thus, our experimental results indicate that H_2O_2 has the hardest penetration ability through the SC layer after plasma treatment, whereas NO_2^- and NO_3^- penetrate more easily through the SC layer. This phenomenon can be caused by two factors: first, H_2O_2 is consumed by the antioxidants in the SC, whereas these antioxidants hardly react with NO_2^- and NO_3^-. Indeed, it was reported that the antioxidant network present in the SC protects the skin from oxidative stress via antioxidants, and the concentration of carotenoids in the SC decreases after plasma treatment.[56] The antioxidants in the SC include carotenoids,[57] vitamin E, vitamin C, glutathione, uric acid, and catalase.[58,59] Thus, these antioxidants can react with H_2O_2, thereby resulting in a lower permeability of

TABLE 1 The blocking effect of the SC on RONS penetration for 20-min plasma treatment

Long-lived species	No SC covered c_2 (µM)	Moist SC covered Concentration c_1 (µM)	Moist SC covered Blocking ratio k_b (%)	Dry SC covered Concentration c_1 (µM)	Dry SC covered Blocking ratio k_b (%)
H_2O_2	285.7 ± 13.3	2.7 ± 0.2	99.1	< 1	~100
NO_3^-	31.6 ± 2.7	4.2 ± 0.2	86.7	3.6 ± 0.3	88.6
NO_2^-	4.3 ± 0.3	2.0 ± 0.1	53.5	1.3 ± 0.1	69.8

Abbreviations: RONS, reactive oxygen and nitrogen species; SC, stratum corneum.

H_2O_2. As is clear from Figures 4a, 5a, and 6a, H_2O_2 is the only species among the investigated substances that exhibits a kind of "delay time" in its permeation behavior. In other words, in the case of moist SC layer, the H_2O_2 concentration in the receiving well remains zero at the beginning and starts to increase only after about 10 min (Figure 4a), whereas other species (NO_2^- and NO_3^-) permeate from the very beginning (see Figures 5a and 6a). Thus, we can assume that there is a high probability of H_2O_2 consumption by antioxidants at the beginning of the experiment. Only after the effect of antioxidants, H_2O_2 manages to pass through the SC layer, thus having, in general, the hardest penetration ability. Second, the SC has a different barrier effect for H_2O_2 molecule than for NO_2^- and/or NO_3^-. This might also be the reason for the higher storage of H_2O_2 than the other species after plasma treatment. This effect will be discussed in detail in Section 4.6.

As we mentioned, after plasma treatment, a lot of RONS are stored in the SC layer, indicating that the SC layer acts as an RONS receiving pool when treated by the plasma, which is also linked with the strong barrier effects of the SC.

4.6 | FEPs of RONS across the SC lipid bilayers

To study the transport of RONS across the SC layer, the FEPs of some typical RONS (H_2O_2, OH, HO_2, O_2, O_3, NO, NO_2, N_2O_4, HNO_2, HNO_3, NO_2^-, and NO_3^-) through the native and oxidized SC lipid bilayers were calculated by means of MD simulations.

The results are presented in Figure 7, and the transfer free energies (ΔG) of the various RONS across the native and oxidized SC lipid bilayers are summarized in Table 2 (ordered from the highest to the lowest values).

The results show that the ions (NO_3^- and NO_2^-) have a Λ-shaped FEP with the highest permeation barriers across the SC lipid bilayers (Figure 7). In nature, ions hardly permeate across the cell lipid membrane by passive diffusion, due to their higher hydration free energies and the strong absorption by the hydrophilic lipid heads,[60] and they always need typical channels (anion transport proteins) to be transported.[61] Similarly, in our SC lipid bilayer, NO_3^- and NO_2^- have the highest transfer free energies (83.05 and 76.71 kJ/mol, respectively), see Table 2. The results also show that NO_3^- and NO_2^- have similar FEPs (see Figure 7), which may result from the special permeation mechanism of ions, called ion-induced, defect-driven permeabilities.[62] Under this permeation mechanism, the interface between the water and lipid bilayer is reshaped due to the force of ions, and ions have similar FEPs, despite the fact that they have different chemical composition, size, and hydration free energy.

The transfer free energies of all other electroneutral species, from water to the center of the lipid bilayer, show a similar profile (see Figure 7a), that is, they first decrease near the water–lipid interface and then increase, reaching their maximum values in the lipid region, followed by a decrease at the center of the bilayer. All hydrophilic species (i.e., H_2O_2, OH, HO_2, HNO_2, and HNO_3)[63] have minimum energies close to the water–lipid interface, which mainly results from the H-bonding and dispersion interactions between these RONS and the head groups of the bilayer.[42,44] The hydrophobic RONS (i.e., O_2, O_3, NO, NO_2, and N_2O_4),[63] however, have their minimum energies (i.e., lower than in water) at the center of the bilayer, except for N_2O_4 that has a slightly higher energy (~1 kJ/mol) than in water (see Figure 7a).

Our simulation results show that the hydrophobic species (O_2, O_3, NO, NO_2, and N_2O_4) have lower barriers than the hydrophilic species (H_2O_2, OH, HO_2, HNO_2, HNO_3) to transport to the bilayer center (see Table 2). Experiments also showed that hydrophilic solutions hardly permeate through the skin layer.[64]

Our experimental results showed that the SC layer has the highest barrier for H_2O_2 penetration, compared with NO_3^- and NO_2^- (see blocking ratios in Table 1). However, our MD simulations show that the transfer free energies of NO_3^- and NO_2^- (i.e., 83.05 and 76.71 kJ/mol) are much bigger than that of H_2O_2 across the native SC lipid bilayers (i.e., 39.59 kJ/mol). This indicates that the NO_3^- and NO_2^- concentrations measured in the receiving wells (in our experiments) are probably not due to NO_3^- and NO_2^- directly penetrating through the SC layer. There are two transform routes that may cause these results: (a) NO_3^- and NO_2^- probably originate from HNO_3 and HNO_2 penetrating through the SC layer. Acids (i.e., HNO_3 and HNO_2) are produced during the plasma treatment and they have a lower barrier for permeation across the SC lipid bilayer, compared with their ionic forms (i.e., NO_3^- and NO_2^-), see Figure 7a. Thus, NO_3^- and NO_2^- measured in the receiving wells may be derived from the penetrations of their acid forms (i.e., HNO_2 and HNO_3). (b) The gaseous RNS (NO and NO_2), which have very low barriers to translocate across the SC lipid bilayer (see Figure 7a), penetrate the SC layer first and then convert into NO_2^- and NO_3^-. NO_2^- and NO_3^- are the final products of Reactions (3) and (4). Further research is needed to verify the contributions of these two pathways.
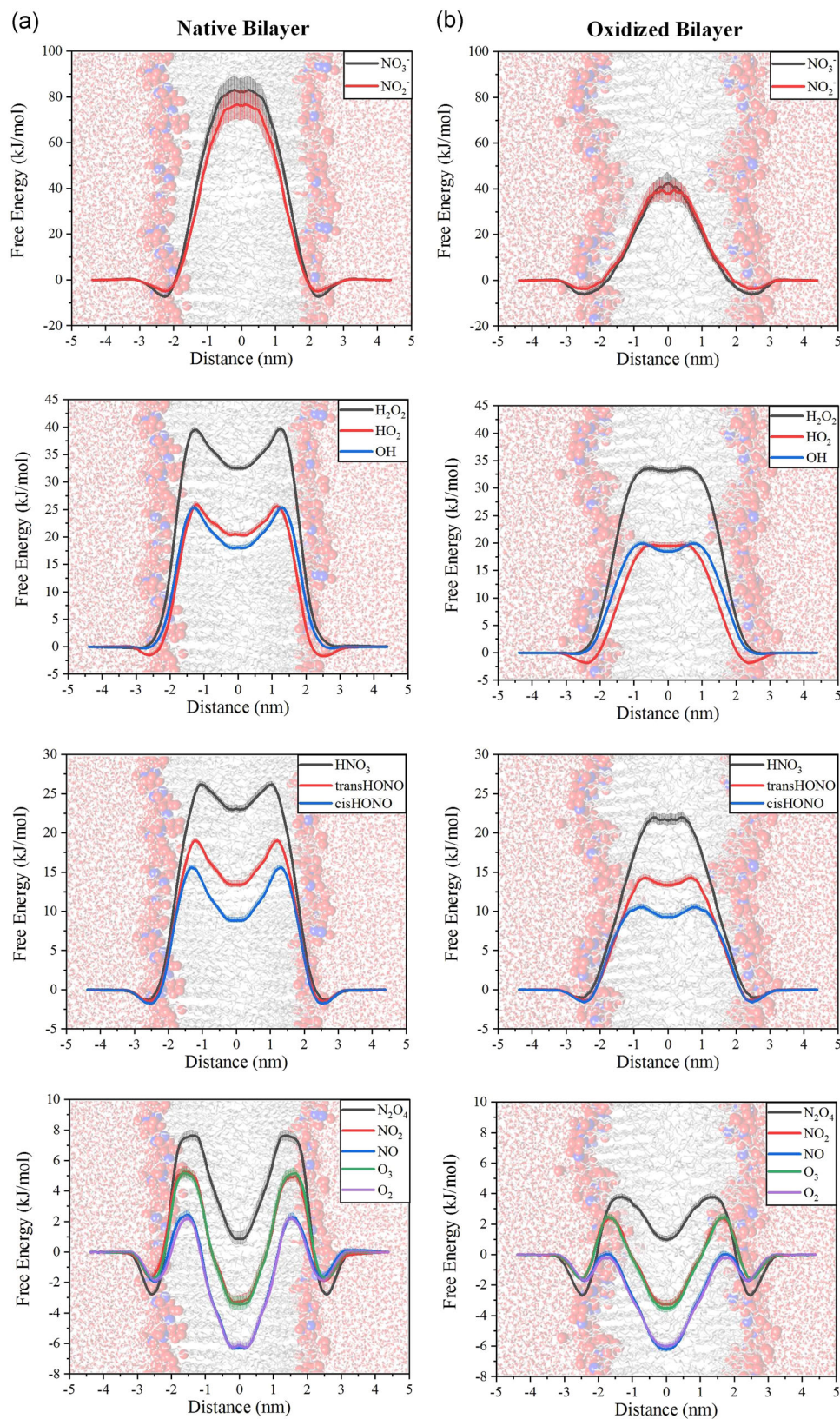
$$NO_2 + NO_2 + H_2O \rightarrow NO_2^- + NO_3^- + 2H^+, \quad (3)$$

$$NO + NO_2 + H_2O \rightarrow 2NO_2^- + 2H^+. \quad (4)$$
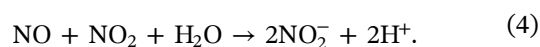
FIGURE 7 Free energy profiles of typical reactive oxygen and nitrogen species (NO_3^-, NO_2^-, H_2O_2, HO_2, OH, HNO_3, HNO_2 [i.e., *trans*-HONO and *cis*-HONO], N_2O_4, NO_2, NO, O_3, O_2) across (a) the native and (b) oxidized stratum corneum lipid bilayers. For clarity, the lipid bilayers are illustrated in the background

TABLE 2 Transfer free energies (ΔG) of RONS across the SC lipid bilayers

	ΔG (kJ/mol)	
Species	**Native**	**Preoxidized**
NO_3^-	83.05 ± 5.82	42.53 ± 4.30
NO_2^-	76.71 ± 6.42	39.49 ± 4.35
H_2O_2	39.59 ± 0.47	33.59 ± 0.52
HNO_3	26.18 ± 0.36	22.00 ± 0.63
OH	25.93 ± 0.34	20.00 ± 0.34
HO_2	25.93 ± 0.49	19.82 ± 0.52
trans-HONO	18.99 ± 0.28	14.30 ± 0.34
cis-HONO	15.58 ± 0.26	10.54 ± 0.32
N_2O_4	7.64 ± 0.33	3.87 ± 0.18
NO_2	5.27 ± 0.31	2.34 ± 0.20
O_3	5.16 ± 0.31	2.46 ± 0.21
NO	2.35 ± 0.18	0.02 ± 0.14
O_2 ($^1O_2$)	2.19 ± 0.17	-0.15 ± 0.14

Abbreviations: RONS, reactive oxygen and nitrogen species; SC, stratum corneum.

Thus, our simulation results indicate that the permeability of typical ROS, like H_2O_2, OH, and HO_2, across the skin lipids, is much lower (due to much higher barriers or transfer free energies) than for typical RNS (NO, NO_2, N_2O_4), O_2, and O_3, indicating that RNS, O_2, and O_3 may play an important role in plasma medicine applications.

4.7 | Penetration of RONS across oxidized SC lipid bilayers

We also investigated the oxidation effect of lipids on the RONS penetration across the SC lipid bilayer by the MD simulations (Figure 7b). In our model, we assumed that all of the CHOs (Figure 3c) are oxidized to 5α-CHs (Figure 3d). Our results show that the oxidation of CHOs leads to a decrease of the permeation barriers of all RONS. Especially, the permeation barriers of the ions (NO_3^- and NO_2^-) are reduced to a larger extent than the other electroneutral species. Thus, in general, RONS penetrate across the SC lipid bilayers more easily when the lipids are oxidized. This is due to the instability of the lipid bilayers caused by oxidization. From Figure 3b, we can clearly observe that the oxidized lipid bilayer loses its highly ordered arrangements. The calculated APL and thickness of the bilayer are presented in Table 3. It is clear that the APL increases and the bilayer thickness

TABLE 3 Average APL and thickness of the native and oxidized bilayer

	APL (nm^2)	Thickness (nm)
Native bilayer	0.340 ± 0.003	4.832 ± 0.259
Oxidized bilayer	0.353 ± 0.005	4.623 ± 0.425

Abbreviation: APL, area per lipid.

decreases as the CHO lipids are oxidized; the interspaces between lipids in the water–lipid interface increase, which results in easier penetrations of RONS across the bilayer.

5 | CONCLUSIONS

Our experimental results indicate that the penetration of RONS across the SC layer increases when the SC layer is moist, compared with the dry SC layer, and our MD simulation results indicate that the permeability of RONS across the SC lipid bilayer is enhanced when the lipids are oxidized. These results may help to increase the effects of cold plasma in medical applications. Moreover, the simulation results indicate that the RNS (NO, NO_2, N_2O_4), O_2, and O_3 penetrate the SC layer more easily than the hydrophilic ROS (H_2O_2, OH, HO_2), which may contribute to a better understanding of the therapeutic effects of the cold atmospheric plasma.

ORCID
Jiangwei Duan http://orcid.org/0000-0003-1213-2804
Maksudbek Yusupov http://orcid.org/0000-0003-4591-858X

REFERENCES
[1] A. Schmidt, S. Bekeschus, K. Wende, B. Vollmar, T. von Woedtke, *Exp. Dermatol.* **2017**, *26*, 156.
[2] J. Gao, L. Wang, C. Xia, X. Yang, Z. Cao, L. Zheng, R. Ko, C. Shen, C. Yang, C. Cheng, *Int. Wound J.* **2019**, *16*, 1103.

[3] A. Schmidt, S. Bekeschus, *Antioxidants* **2018**, *7*, 146.

[4] T. Bernhardt, M. L. Semmler, M. Schäfer, S. Bekeschus, S. Emmert, L. Boeckmann, *Oxid. Med. Cell. Longevity* **2019**, *2019*, 10.

[5] L. Gan, J. Duan, S. Zhang, X. Liu, D. Poorun, X. Liu, X. Lu, X. Duan, D. Liu, H. Chen, *Free. Radic. Res.* **2019**, *53*, 1.

[6] H.-R. Metelmann, C. Seebauer, V. Miller, A. Fridman, G. Bauer, D. B. Graves, J.-M. Pouvesle, R. Rutkowski, M. Schuster, S. Bekeschus, K. Wende, K. Masur, S. Hasse, T. Gerling, M. Hori, H. Tanaka, E. H. Choi, K.-D. Weltmann, P. H. Metelmann, D. D. Von Hoff, T. von Woedtke, *Clin. Plasma Med.* **2018**, *9*, 6.

[7] M. Ma, J. Duan, X. Lu, G. He, *Phys. Plasmas* **2019**, *26*, 23523.

[8] M. Keidar, D. Yan, I. I. Beilis, B. Trink, J. H. Sherman, *Trends Biotechnol.* **2018**, *36*, 586.

[9] X. Lu, G. V. Naidis, M. Laroussi, S. Reuter, D. B. Graves, K. Ostrikov, *Phys. Rep.* **2016**, *630*, 1.

[10] S. Hasse, T. Duong Tran, O. Hahn, S. Kindler, H.-R. Metelmann, T. von Woedtke, K. Masur, *Clin. Exp. Dermatol.* **2016**, *41*, 202.

[11] A. Schmidt, S. Bekeschus, T. von Woedtke, S. Hasse, *Clin. Plasma Med.* **2015**, *3*, 24.

[12] S. J. Kim, T. H. Chung, *Sci. Rep.* **2016**, *6*, 20332.

[13] J. Duan, X. Lu, G. He, *J. Appl. Phys.* **2017**, *121*, 13302.

[14] M. Yusupov, K. Wende, S. Kupsch, E. C. Neyts, S. Reuter, A. Bogaerts, *Sci. Rep.* **2017**, *7*, 5761.

[15] L. Guo, Y. Zhao, D. Liu, Z. Liu, C. Chen, R. Xu, M. Tian, X. Wang, H. Chen, M. G. Kong, *Free. Radic. Res.* **2018**, *52*, 783.

[16] A. M. Hirst, M. S. Simms, V. M. Mann, N. J. Maitland, D. O'Connell, F. M. Frame, *Br. J. Cancer* **2015**, *112*, 1536.

[17] S. Bekeschus, A. Schmidt, L. Bethge, K. Masur, T. von Woedtke, S. Hasse, K. Wende, *Oxid. Med. Cell. Longevity* **2016**, *2016*, 11.

[18] N. K. Kaushik, N. Kaushik, B. Min, K. H. Choi, Y. J. Hong, V. Miller, A. Fridman, E. H. Choi, *J. Phys. D: Appl. Phys.* **2016**, *49*, 84001.

[19] A. Lin, B. Truong, G. Fridman, A. A. Fridman, V. Miller, *Plasma Med.* **2017**, *7*, 85.

[20] E. J. Szili, J.-S. Oh, H. Fukuhara, R. Bhatia, N. Gaur, C. K. Nguyen, S.-H. Hong, S. Ito, K. Ogawa, C. Kawada, *Plasma Sources Sci. Technol.* **2017**, *27*, 014001.

[21] T. Haque, M. M. U. Talukder, *Adv. Pharm. Bull.* **2018**, *8*, 169.

[22] C. R. Harding, *Dermatol. Ther.* **2004**, *17*, 6.

[23] J. van Smeden, J. A. Bouwstra, *Curr. Probl. Dermatol.* **2016**, 8.

[24] G. K. Menon, G. W. Cleary, M. E. Lane, *Int. J. Pharm.* **2012**, *435*, 3.

[25] C. Das, G. N. Massimo, D. O. Peter, *Biophys. J.* **2009**, *97*, 1941.

[26] R. Notman, J. Anwar, *Adv. Drug Delivery Rev.* **2013**, *65*, 237.

[27] M. Lundborg, C. L. Wennberg, A. Narangifard, E. Lindahl, L. Norlén, *J. Controlled Release* **2018**, *283*, 269.

[28] M. N. Al-Qattan, P. K. Deb, R. K. Tekade, *Drug Discovery Today* **2018**, *23*, 235.

[29] J. Torin Huzil, S. Sivaloganathan, M. Kohandel, M. Foldvari, *Wiley Interdiscip. Rev.: Nanomed. Nanobiotechnol.* **2011**, *3*, 449.

[30] X. Lu, M. Keidar, M. Laroussi, E. Choi, E. J. Szili, K. Ostrikov, *Mater. Sci. Eng., R* **2019**, *138*, 36.

[31] U. Jacobi, M. Kaiser, R. Toll, S. Mangelsdorf, H. Audring, N. Otberg, W. Sterry, J. Lademann, *Ski. Res. Technol.* **2007**, *13*, 19.

[32] C. Herkenne, A. Naik, Y. N. Kalia, J. Hadgraft, R. H. Guy, *Pharm. Res.* **2006**, *23*, 1850.

[33] Y. Yang, Z. Li, L. Nie, X. Lu, *J. Appl. Phys.* **2019**, *125*, 223302.

[34] J. Duan, L. Gan, L. Nie, F. Sun, X. Lu, G. He, *Phys. Plasmas* **2019**, *26*, 43504.

[35] S. Kumar, D. K. Yadav, E. H. Choi, M. H. Kim, *Sci. Rep.* **2018**, *8*, 1.

[36] D. K. Yadav, S. Kumar, E.-H. Choi, P. Sharma, S. Misra, M.-H. Kim, *Front. Pharmacol.* **2018**, *9*, 644.

[37] L. Martínez, R. Andrade, E. G. Birgin, J. M. Martínez, *J. Comput. Chem.* **2009**, *30*, 2157.

[38] M. J. Abraham, T. Murtola, R. Schulz, S. Páll, J. C. Smith, B. Hess, E. Lindahl, *SoftwareX* **2015**, *1–2*, 19.

[39] O. Berger, O. Edholm, F. Jähnig, *Biophys. J.* **1997**, *72*, 2002.

[40] M. Höltje, T. Förster, B. Brandt, T. Engels, W. von Rybinski, H.-D. Höltje, *Biochim. Biophys. Acta, Biomembr.* **2001**, *1511*, 156.

[41] A. J. P. Neto, R. M. Cordeiro, *Biochim. Biophys. Acta, Biomembr.* **2016**, *1858*, 2191.

[42] R. M. Cordeiro, *Biochim. Biophys. Acta, Biomembr.* **2014**, *1838*, 438.

[43] R. M. Cordeiro, *J. Phys. Chem. B* **2018**, *122*, 8211.

[44] J. Razzokov, M. Yusupov, R. M. Cordeiro, A. Bogaerts, *J. Phys. D: Appl. Phys.* **2018**, *51*, 365203.

[45] R. M. Cordeiro, M. Yusupov, J. Razzokov, A. Bogaerts, *J. Phys. Chem. B* **2020**, *124*, 1082.

[46] J. S. Hub, B. L. de Groot, D. van der Spoel, *J. Chem. Theory Comput.* **2010**, *6*, 3713.

[47] W. J. Allen, J. A. Lemkul, D. R. Bevan, *J. Comput. Chem.* **2009**, *30*, 1952.

[48] J. Winter, H. Tresp, M. U. Hammer, S. Iseni, S. Kupsch, A. Schmidt-Bleker, K. Wende, M. Duennbier, K. Masur, K.-D. Weltmannan, S. Reuter, *J. Phys. D: Appl. Phys.* **2014**, *47*, 285401.

[49] P. Bruggeman, D. C. Schram, *Plasma Sources Sci. Technol.* **2010**, *19*, 45025.

[50] J. Winter, K. Wende, K. Masur, S. Iseni, M. Dünnbier, M. U. Hammer, H. Tresp, K.-D. Weltmann, S. Reuter, *J. Phys. D: Appl. Phys.* **2013**, *46*, 295401.

[51] X. Liu, L. Gan, M. Ma, S. Zhang, J. Liu, H. Chen, D. Liu, X. Lu, *J. Phys. D: Appl. Phys.* **2018**, *51*, 75401.

[52] H. Zhai, H. I. Maibach, *Skin Pharmacol. Appl. Skin Physiol.* **2001**, *14*, 1.

[53] Y. Gorbanev, A. Privat-Maldonado, A. Bogaerts, *Anal. Chem.* **2018**, *90*, 13151.

[54] U. Förstermann, W. C. Sessa, *Eur. Heart J.* **2011**, *33*, 829.

[55] D. Tousoulis, A.-M. Kampoli, C. Tentolouris Nikolaos Papageorgiou, C. Stefanadis, *Curr. Vasc. Pharmacol.* **2012**, *10*, 4.

[56] J. W. Fluhr, S. Sassning, O. Lademann, M. E. Darvin, S. Schanzer, A. Kramer, H. Richter, W. Sterry, J. Lademann, *Exp. Dermatol.* **2012**, *21*, 130.

[57] J. Lademann, S. Schanzer, M. Meinke, W. Sterry, M. E. Darvin, *Skin Pharmacol. Physiol.* **2011**, *24*, 238.

[58] J. J. Thiele, C. Schroeter, S. N. Hsieh, M. Podda, L. Packer, *Oxidants and Antioxidants in Cutaneous Biology*, Vol. 29, Karger, Basel **2001**, pp. 26–42.

[59] J. J. Thiele, *Skin Pharmacol. Physiol.* **2001**, *14*, 87.

[60] A. P. Davis, D. N. Sheppard, B. D. Smith, *Chem. Soc. Rev.* **2007**, *36*, 348.

[61] A. J. Miller, X. Fan, M. Orsel, S. J. Smith, D. M. Wells, *J. Exp. Bot.* **2007**, *58*, 2297.

[62] I. Vorobyov, T. E. Olson, J. H. Kim, R. E. Koeppe, O. S. Andersen, T. W. Allen, *Biophys. J.* **2014**, *106*, 586.

[63] R. Vácha, P. Slavíček, M. Mucha, B. J. Finlayson-Pitts, P. Jungwirth, *J. Phys. Chem. A* **2004**, *108*, 11573.

[64] L. Chen, L. Han, G. Lian, *Adv. Drug Delivery Rev.* **2013**, *65*, 295.